

SIM Internal Metrology Beam Launcher Development

Feng Zhao*, Rosemary Diaz, Gary Kuan, Norbert Sigrist, and Yuri Beregovski
 Jet Propulsion Laboratory, Pasadena, California 91109
 Lawrence Ames, and Kalyan Dutta
 Lockheed Martin Advanced Technology Center, Palo Alto, California 94304

ABSTRACT

To accomplish micro-arcsecond astrometric measurement, stellar interferometers such as SIM require the measurement of internal optical path length delay with an accuracy of ~ 10 picometers level. A novel common-path laser heterodyne interferometer suitable for this application was proposed and demonstrated at JPL. In this paper, we present some of the experimental results from a laboratory demonstration unit and design considerations for SIM's internal metrology beam launcher.

Keywords: interferometry, metrology, laser heterodyne interferometers, astrometry

1 INTRODUCTION

The Space Interferometry Mission (SIM) is a space-based optical Michelson interferometer with its primary goal of measuring positions and motions of celestial objects. In its simplest form, SIM performs relative astrometry between two stars by taking a pair of internal optical path length delay measurements: one for each star in turn, as shown in Figure 1. The two delay-line positions are located by searching for the maximum fringe amplitude on each star. A key measured quantity is the change in internal delay Δd ,

$$\Delta d = \bar{B} \cdot (\bar{s}_1 - \bar{s}_2),$$

where \bar{B} is the baseline vector (length and orientation) and \bar{s}_1 and \bar{s}_2 are unit vectors to the two stars. The angular distance between the two stars ($\bar{s}_1 - \bar{s}_2$) can then be calculated once Δd and \bar{B} are known. The job of internal metrology is to measure Δd . For SIM, Δd must be measured with an accuracy on the order of 10 picometers in order to achieve 1 microarcsecond astrometry with a 10m baseline.

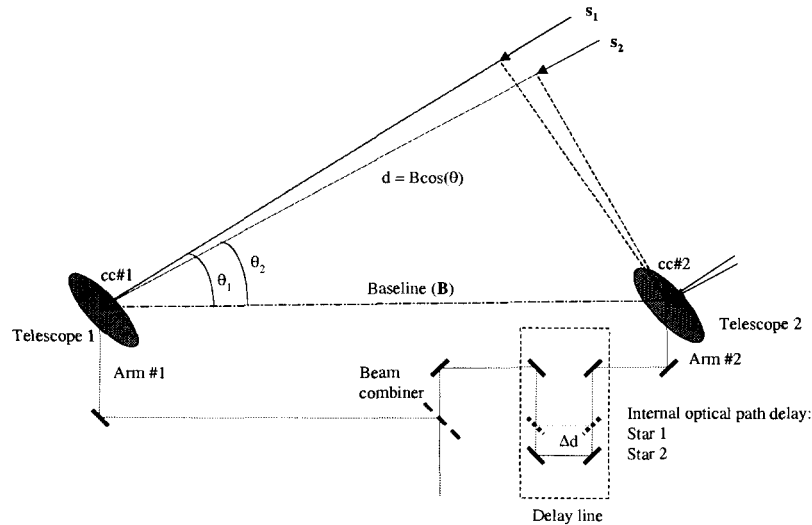


Figure 1. Stellar interferometer for astrometric measurement. The internal delay Δd between two star central fringes gives the angular distance between the two stars.

* Feng.Zhao@jpl.nasa.gov; phone (818)354-3602; fax (818)393-2412, Jet Propulsion Laboratory, M/S 301-486, California Institute of Technology, 4800 Oak Grove Drive, Pasadena, California 91109

Laser heterodyne interferometers have been widely used in high precision displacement measurement and also have been the choice for stellar interferometry for measuring internal path delays [1]. Commercial available heterodyne interferometers are limited to about 1-2nm in linear accuracy [2]. The well-known error term is cyclic error which happens every integer number $\lambda/2$ of displacement in most of the configurations. The cyclic error has been a subject of intensive research [2], and some interesting concepts have been demonstrated to beat the cyclic error down to below 100pm level [3]. However, these concepts are not suited for use in SIM because they are intrinsically sensitive to temperature changes.

A novel COMmon-Path Heterodyne Interferometer (COPHI) was proposed at JPL as a multi-purpose, high resolution laser interferometer [4-6]. Experimental results indicated that very low cyclic error (27pm RMS) and good thermal stability (100pm over one hour) can be obtained at the same time with COPHI [6]. In this paper, we will first describe the COPHI concept and its use as internal metrology beam launcher* for SIM. We will also present some experimental results of one of our laboratory prototypes. In Section 4, we will present some analysis and design work toward a flight internal metrology beam launcher for SIM.

2 COMMON-PATH HETERODYNE INTERFEROMETER (COPHI)

Figure 2 shows COPHI configured as a displacement measuring inerferometer for internal path length measurement. It is a laser heterodyne interferometer, where two laser beams with a frequency offset Δf are collimated with stable collimators. One beam is directed to the measurement target with a beam splitter (the top beam at frequency f_o in Figure 2). The interferometer is located at the back end of the astrometric beam combiner, so that the measurement beam passes through the beam combiner and travels toward the star. We place a pair of masks after the beam combiner, one in each arm. The two masks are complimentary, with one selecting only the central portion of the measurement beam, while the other mask selecting an annular part of the beam. As shown in Figure 2, the central beam travels in Arm #2 and the annular beam travels in Arm #1. These two beams are then retro-reflected back to the interferometer by corner cubes #1 and #2, respectively. These two measurement beams are spatially separated with a guard band to reduce cross-talk contamination due to diffraction. The second laser beam (reference beam) at frequency $f_o + \Delta f$, which serves as a local oscillator, then interferes with both measurement beams at the second beam splitter. The two spatially separated fringes are then directed to their own photodiodes with the use of a truncated mirror. The phase difference ($\Delta\phi$) between the reference and measurement signals

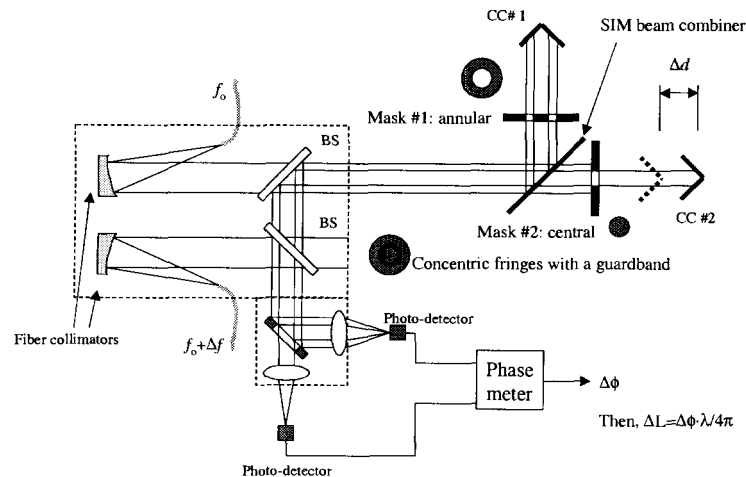


Figure 2. Schematic of a common-path heterodyne interferometer, configured for internal path length measurement.

* The term “beam launcher” refers to laser interferometer for path length measurement in SIM.

is then used to calculate the displacement (Δd) between the fiducials:

$$\Delta d = \frac{\Delta\phi}{2\pi} \frac{\lambda}{2},$$

where λ is the laser wavelength.

One obvious advantage of using COPHI is that the internal path delay is measured directly with only one interferometer. In conventional internal path length measurement, two interferometers are used to measure the path length in two arms separately [1]. The internal path delay is then the difference of the two measurements. Two sets of phase measurement electronics are needed. The use of COPHI to measure internal path delay reduces the number of beam launchers and the number of phase measurement electronics to only one set.

The second advantage of using COPHI for internal path delay measurement is that the alignment process of the stellar interferometer becomes simpler. To measure the starlight path length accurately, the laser metrology beam and starlight beam must be parallel and the beams from Arm #1 and Arm #2 must be parallel at the astrometric beam combiner, both to be better than $1\mu\text{rad}$. Since the measurement beams from COPHI are derived from the same collimated wavefront, they are intrinsically parallel. This feature reduces the number of precise alignments in SIM. It also makes it possible to use the COPHI beams as an alignment reference for pointing the two starlight arms.

COPHI also has much smaller nonlinear errors as compared with traditional interferometers. The once largest error source for cyclic error, namely polarization leakage is no longer an issue in COPHI. Since the wavefronts are spatially separated, diffraction may cause crosstalk, thus cyclic error in the measurement. Practically, several simple methods such as baffle to isolate the beams, re-imaging of the mask onto truncated mirror, etc. are quite effective. In addition to these measures, the local oscillator serves as a "spatial filter", which further rejects the contribution of stray light when interfering with the measurement beams. This is because the diffracted beam tends to have a high angular frequency, therefore poor fringe visibility when interfering with a clean local oscillator reference beam. Both analysis and laboratory demonstration have confirmed that the diffraction induced cyclic error can be controlled to 10pm level with a proper guard band between the two wavefront portions. This represents about a factor of 100 in improvement over traditional interferometers.

In COPHI, the wavefront of the measurement beam is split into two symmetric portions, with minimum lateral offset between the two beams. They are referenced to the same reference beam (the local oscillator). The two signals are common-path except that they pass through different parts of the same optics. Therefore, good thermal stability can be achieved without using any compensating optics.

3 LABORATORY DEMONSTRATION

In the last two years, we have designed, built and tested several laboratory prototypes based on COPHI concept for various testbeds [6-9]. In this section, we will describe the SAVV (sub-aperture vertex to vertex) interferometer we developed for the Micro-Arcsecond Metrology (MAM) testbed at JPL.

MAM testbed is part of SIM technology development program aimed at demonstrating micro-arcsecond astrometry, i.e., picometer path length measurement in a laboratory environment. Internal metrology based on traditional polarization type interferometers in MAM has proved to be much more difficult than anticipated [10-12]. SAVV was proposed to address the urgent need for picometer class path length measurement in MAM in late 2000. The first prototype was built with commercial off-the-shelf (COTS) optics.

Figures 3 and 4 show the schematic layout and picture of the first SAVV interferometer. Commercial off-the-shelf doublet collimating lenses are used to collimate the laser beams. To minimize thermal drift error caused by collimator de-spacing, we use a four-quadrant mask pattern, as shown in Figure 5. The collimator de-spacing then becomes a common-mode error, because the measurement beams are on the same radius. The vertical pair and horizontal pair are used in the two arms of the MAM interferometer, selected by a pair of masks shown in Figure 6. Because the diffraction is minimum along the diagonals in the square mask, we select square beam patterns for each beam. Therefore, crosstalk between the vertical and horizontal pairs also becomes minimum. A pair of Risley prisms are used in fine alignment ($1\mu\text{rad}$) of the reference beam (local oscillator) to be parallel to the measurement beams. Two

picomotor rotary stages (New Focus) are used to achieve fine adjustment and also remote alignment to correct for any drift when the interferometer is used in vacuum.

The cyclic error of SAVV was measured with a standard linear long stroke approach, in which one of the two corner cubes was translated with a PZT. The linear path length modulation is much longer than one wavelength, therefore, any cyclic error can be detected by looking at the power spectrum of the displacement result. In our experiment, the laser wavelength is $1.319 \mu\text{m}$, and the total stroke of the PZT is about $40 \mu\text{m}$ with a triangle wave modulation at 0.05Hz . Thus cyclic error with $\lambda/2$ periodicity can be found at about 3.5Hz in the spectral domain.

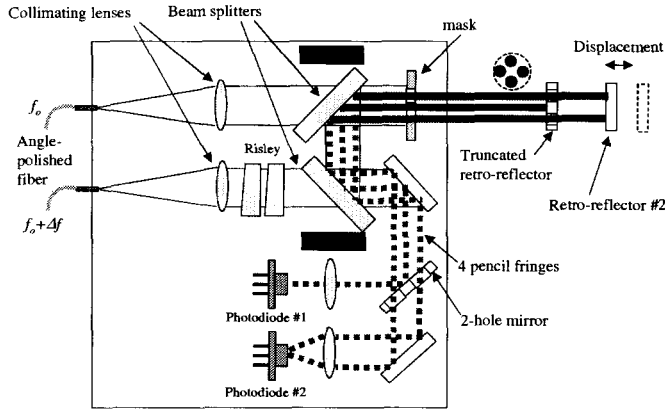


Figure 3. SAVV schematic.

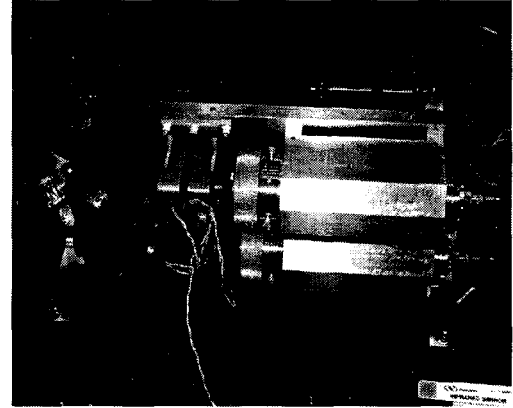


Figure 4. Picture of a SAVV prototype interferometer.

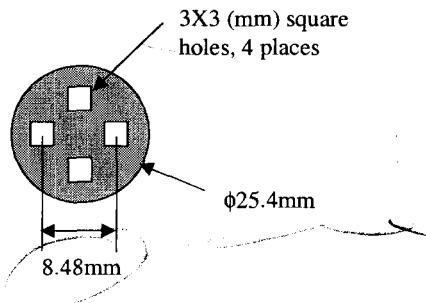


Figure 5. Four square beams are selected from the collimated beam with a quadrant mask in SAVV.

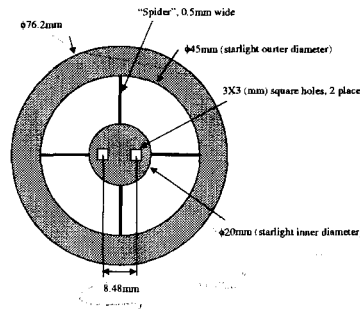


Figure 6. A two-hole mask in Arm #1 selects a horizontal pair of the quadrant beams. In Arm #2, an identical mask rotated by 90 degrees selects the vertical beams. The 20mm central obscuration in starlight is used for laser metrology for path delay measurement

Figure 7-a shows the measured displacement of the PZT. We select an arbitrary linear displacement, e.g., between 44 and 61 seconds in Figure 7 for analysis. Figure 7-b shows its residual after removing its linear to 4th order terms. The power spectral density of the residual is calculated and plotted in Figure 8-a, in which the peak at 3.8Hz indicates the existence of $\lambda/2$ periodic nonlinear error. The total energy of this cyclic error is estimated to be about 4500pm^2 , which translates into a periodic nonlinear error of only 67pm RMS (figure 8-b). This result exceeds MAM's requirement for 100pm cyclic error.

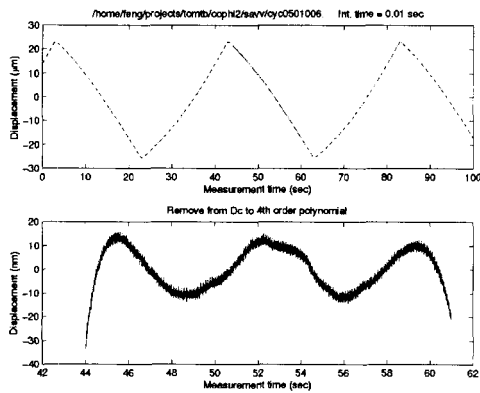


Figure 7. Linear displacement over many laser wavelengths to detect cyclic error in SAVV. The bottom plot shows the residual after removing its DC to 4th order polynomial terms.

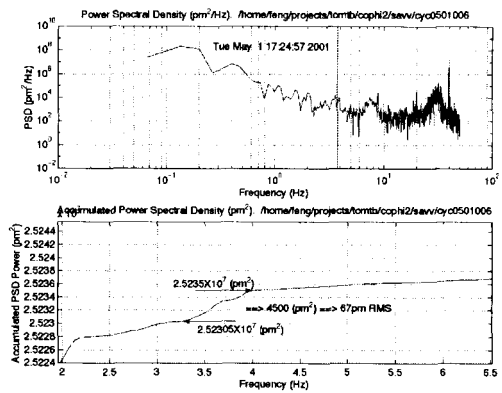


Figure 8. Power spectral density of Figure 7-b. The peak at 3.8Hz is attributed to SAVV cyclic error. The accumulated PSD data (bottom) indicates the cyclic error is about 67pm RMS.

The cyclic error measurement result was then checked against wave optics diffraction model. In the model, the diffraction effects of both beams at various mask apertures are calculated. Diffraction results in cross-talk between the two photo detectors, which in turn causes error in average phase of each signal. The calculated cyclic error in the SAVV measurement setup is plotted in Figure 9. The calculations indicate that the cyclic error of SAVV beam launcher is less than 10 pm RMS. The difference between the measurement and calculation may be attributed to other sources of cyclic error such as electronics cross-talk between the two signals, fiber tip back scattering causing a contamination of the two measurement beams, and alignment errors in SAVV.

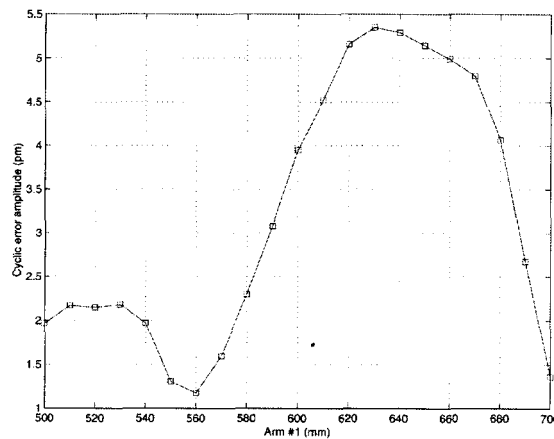


Figure 9. Calculated cyclic error for the SAVV measurement setup. This calculation assumes perfect alignment and considers only the effect of diffraction.

SAVV's temperature sensitivity was measured, using the lab ambient temperature fluctuation ($\sim 1^\circ\text{C}$) as a source to drive SAVV temperature. In the measurement, a corner cube was placed in front of SAVV, all four beams are reflected from this corner cube. Sending all the measurement beams to the same corner cube ensures no path length drift in the fiducial. Thus, any errors in the readout can be attributed to the interferometer. The thermal stability results are shown in Figures 10 and 11. The results indicate that SAVV even built with COTS, has a good thermal stability, less than 4nm/K at room temperature. It can also be seen from Figure 10 that, SAVV drift is highly correlated with the change in temperature gradient.

Gradient fluctuations in the middle of the measurement were caused by the air conditioning on/off in the lab. The flight environment will not have this type of temperature fluctuations.

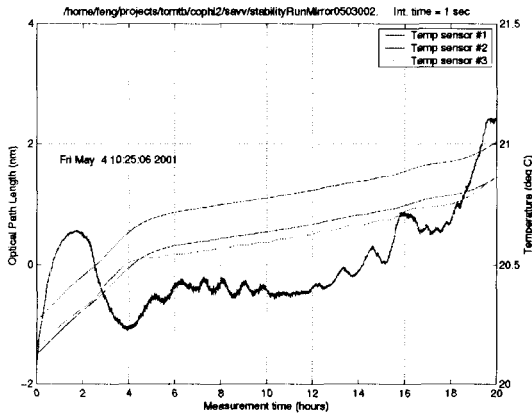


Figure 10. SAVV drift vs. bulk temperature.

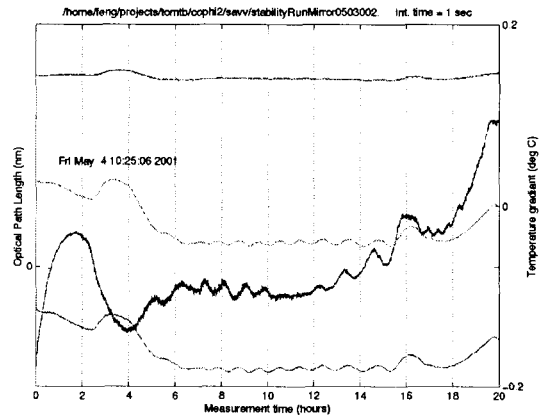


Figure 11. SAVV drift vs. temperature gradient.

4 DESIGN CONSIDERATIONS FOR SIM

The COPHI concept has been successfully demonstrated in ground testbeds and it has been selected as the baseline concept for SIM flight internal metrology. In this section, we will present some of the design considerations for a flight SIM internal metrology interferometer.

One of the differences between ground testbeds (e.g., MAM) and SIM is the total path length that metrology beams and starlight travel. In MAM, the star light path length is 5 meters, and in SIM the path length is about 10-20 meters. In addition, there will be a beam compressor in SIM, where the metrology beam will be magnified by 7 \times . Due to diffraction over long path lengths, the metrology beam expands and requires a relatively large corner cube on the siderostat (SID). On the other hand, a small corner cube is preferred to meet the starlight throughput requirement. Therefore, the flight internal metrology beam size becomes an important aspect of the SIM beam launcher design.

In addition to the beam size constraints set by the corner cube size, the throughput is also an important issue. The four-quadrant beam configuration in MAM internal metrology has the drawback of low light efficiency, since only a few percent of the light is used in the four-quadrant from the collimated beam.

In SIM internal metrology, we plan to use the COPHI configuration, with concentric beams, an annulus and a core, as we described in Section 2 in Figure 2. The layout of SIM internal beam launcher is shown in Figure 12. Low thermal expansion materials such as Zerodur or ULE are used to make the collimator optics (off-axis parabolas and spacers) to ensure thermal stability of the collimated beams. De-spacing of the collimator will cause a focus error in the wavefront, thus an error between the core and annular beams. To some extent, this is a common-mode error, since both collimators will experience similar amount of de-space to thermal soak fluctuations.

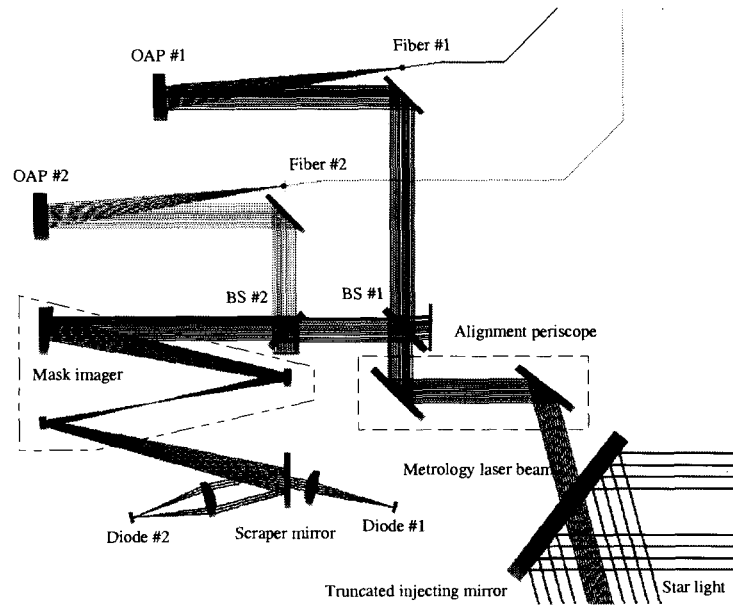


Figure 12. Schematic of internal metrology beam launcher for SIM. The astrometric beam combiner optic and the masks that separate the measurement beams into core and annulus portions are at the lower right corner (not shown).

The SIM internal metrology launcher is located inside of the Astrometric Beam Combiner (ABC), where a truncated mirror behind the main beam combiner optics is used to inject the internal metrology measurement beams into the starlight optics train [13]. The truncated mirror reflects the annular starlight to the starlight camera. A pair of alignment mirrors (periscope) are used to align the metrology beam with the starlight, both in pointing and in overlap. It is much easier to actuate the alignment mirrors than to actuate the beam launcher or starlight optics. After the metrology measurement beam enters the main beam combiner, the beam is then spatially selected into a core beam and an annulus beam separately into two starlight arms with the use of a pair of concentric masks. These two spatially separated beams then propagate along each arm of the starlight optics. Upon reflecting off the corner cubes, the two measurement beams return to the ABC and enters internal beam launcher. The local oscillator beam (fiber #2) is aligned with both the core and annulus measurement beams at the second beam splitter (BS #2). Before the two measurement beams are combined at the beam combiner, they propagate independently in each arm of SIM. The beam diffraction does not introduce cross-talk between them. After returning to the masks at the beam combiner (ABC), the two measurement beams co-propagate and diffraction will cause cross-talk. This happens only between the masks and the scraper mirror, which we use to separate the two fringes. To beat the cyclic error down to the 10pm level, one needs the cross-talk to be less than -80dB . To “reverse” the diffraction effect, we use an imaging system whose two conjugates are the masks and the scraper mirror. By using the imaging approach, the two fringes are separated with smaller cross-talk, thus lower cyclic error. In Figure 12, the “mask imager” is a 3-element, all-spherical, reflective, $1\times$ imaging system. The effects of aberration, aperture, and scattering to fringe cross-talk are now under detailed study.

As mentioned previously, the SID corner cube clear aperture places an upper limit on the metrology beam diameter. If one collimates the measurement beam to infinity, then the beam diameter may be larger than the corner cube. In the SIM internal metrology launcher, we propose to “focus” the laser beams on the SID corner cube. In other words, instead of collimating the laser beams to infinity (finite-to-infinite conjugates), we align the fibers in the collimator to form finite-to-finite conjugates. By doing so, the beam waist where the smallest beam diameter occurs is located at the SID corner cube. Figures 13 and 14 shows an example of beam profiles at different locations. The path length used in this calculation is 8m single-pass. The final path length in SIM is yet to be defined. From the plots, we can see that the core beam

has less diffraction rings, whereas the annulus beam has more diffraction rings due to the inner and out apertures. Both the core and annulus beams have a smaller footprint on the SID corner cube. Upon returning back to the ABC, the diffraction rings are cleaned up by the masks at the beam combiner (ABC). With the use of mask imager, the beam profiles at the scraper mirror look nice and clean (Figure 15).

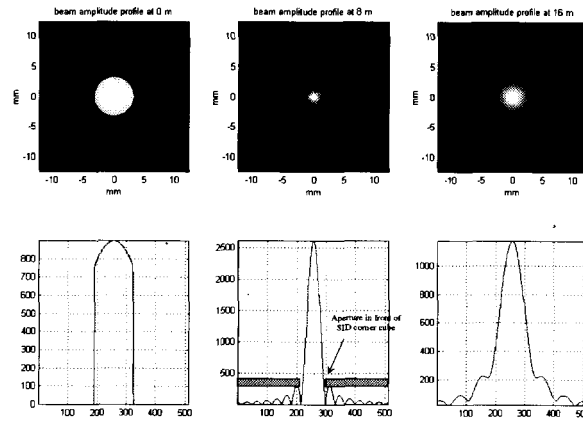


Figure 13. Beam intensity profiles of the core beam at several distances. Left: after the ABC masks traveling to SID. Center: at the SID. Note the clear aperture of the corner cube selects only the central portion of the diffracted beam. Right: back to the ABC masks after a round trip.

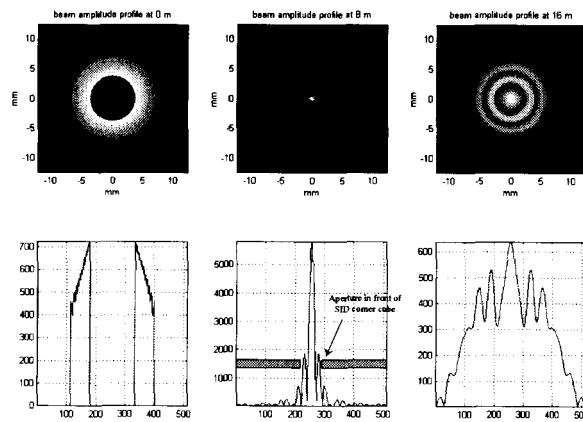


Figure 14. Beam intensity profiles of the annulus beam at several distances. Left: after the ABC masks traveling to SID. Center: at the SID. Note the annulus beam focuses into a smaller spot on SID corner cube. Right: back to the ABC masks after a round trip.

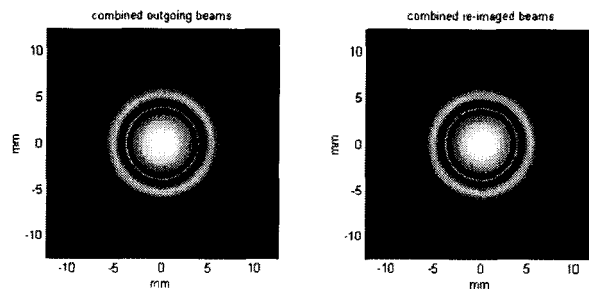


Figure 15. Co-propagating core and annulus beams. Left: after the round trip and combined at the astrometric beam combiner. Right: image at the scraper mirror with the use of mask imager.

The effect of using “finite-to-finite” conjugate ratio in the collimator has a large impact on the beam size on SID corner cube. It allows us to use smaller corner cube on SID, thus improve the starlight throughput. Then the question arises: does the focused beam introduce any error in the average phase in the metrology beam as the path length varies? To answer this question, we have calculated the effect using wave optics diffraction model. The analysis results are plotted in Figure 15, where for both cases, focused and unfocused, there is a quasi-linear deviation from geometric distances. The deviation from geometric case is caused by the fact that both beams have finite beam sizes, thus diffraction occurs in both focused and unfocused beams. This diffraction-induced term in path length measurement is a subject of other papers [14], and readers are referred to the calibration of this term for SIM. In Figure 15, the two traces for focused and unfocused beams have some differences, but there is no effect on how the calibration will be carried out in SIM.

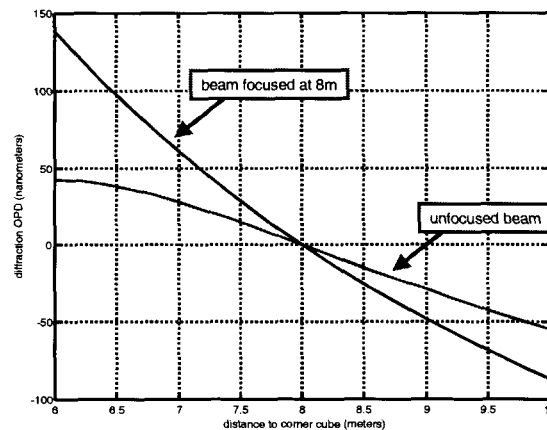


Figure 16. Deviation from geometric distances due to diffraction in both focused and unfocused measurement beams. The horizontal axis represents the internal delay positions.

5 SUMMARY

We have developed and demonstrated an internal metrology beam launcher concept for the Space Interferometry Mission. The concept is based on common-path heterodyne interferometer (COPHI) developed at JPL. The use of spatial separation of measurement beams significantly reduces the cyclic error. Experimental results from laboratory demonstration units have shown encouraging results (cyclic error ~ 67 pm RMS). Calculations based on wave optics diffraction model also indicate that the diffraction in spatially separated measurement beams results in ~ 10 pm level cyclic error. We have also identified a simple approach to reduce the beam sizes over long distances due to diffraction.

ACKNOWLEDGEMENT

The authors would like to thank Jeff Oseas for his help on creating the Light Tool model of the internal metrology beam launcher. This work was carried out at the Jet Propulsion Laboratory, California Institute of Technology, under a contract with the National Aeronautics and Space Administration.

REFERENCES

1. M. Shao, M. M. Colavita, B. E. Hines, D. H. Staelin, D. J. Hutter, K. J. Johnson, D. Mozurkewich, R. S. Simon, J. L. Hersey, J. A. Hughes, and G. H. Kaplan, “Mark III Stellar Interferometer,” *Astron. Astrophysics*, **193**, pp. 357–371, 1988.
2. N. Bobroff, “Recent advances in displacement measuring interferometry”, *Meas. Sci. Technol.*, vol. 4, pp. 907-926, 1993.
3. C.-M. Wu, J. Lawall, R. D. Deslattes, “Heterodyne Interferometer with Subatomic Periodic Nonlinearity”, *Appl. Opt.*, Vol. 38, Issue 19, pp. 4089-4094, 1999.

4. F. Zhao, "A common-path, multi-channel heterodyne interferometer," *NASA Tech. Briefs*, Vol. 25, No. 7, pp12, 2001.
5. F. Zhao, "Interferometric apparatus for ultra-high precision displacement measurement", US Patent Pending, NASA Case No. NPO-21221-1-CU, 2001.
6. F. Zhao, "Demonstration of sub-Angstrom cyclic nonlinearity using wavefront-division sampling with a common-path laser heterodyne interferometer", *Proceeding of the American Society for Precision Engineering (ASPE) Annual Meeting*, Crystal City, VA, 2001.
7. F. Zhao, J. Logan, S. Shaklan, and M. Shao, "A common-path, multi-channel heterodyne laser interferometer for sub-nanometer surface metrology," *Proc. SPIE*, Vol. 3740, pp 642-645, 1999.
8. F. Zhao, R. T. Diaz, P. G. Halverson, G. M. Kuan, and S. Shaklan, "Wavefront versus amplitude division high precision displacement measuring interferometers," *Proceedings of Optoelectronic Distance/Displacement Measurements and Applications (ODIMAP II)*, Pavia, Italy, September 20–22, 2001.
9. F. Zhao, R. T. Diaz, P. Dumont, P. G. Halverson, S. Shaklan, R. E. Spero, L. Ames, S. Barrett, R. Barrett, R. Bell, R. Benson, G. Cross, K. Dutta, T. Kvamme, B. Holmes, D. Leary, P. Perkins, M. Scott, and D. Stubbs, "Development of Sub-nanometer Racetrack Laser Metrology for External Triangulation Measurement for the Space Interferometry Mission," *American Society of Precision Engineering Annual Meeting*, Arlington, VA, November 10–15, 2001
10. A. Kuhnert, S. Shaklan, Y. Gursel, S. Azevedo, and Y. Lin, "Metrology for the micro-arcsecond metrology testbed," *Proceedings of SPIE conference on Astronomical Interferometry*, Vol. 3350, pp. 571–587, 1998.
11. P. G. Halverson, A. Kuhnert, J. Logan, M. Regher, S. Shaklan, R. Spero, F. Zhao, T. Chang, R. Gutierrez, E. Schmitdlin, T. Vanzandt, J. Yu, "Progress toward picometer accuracy laser metrology for the Space Interferometry Mission," *Proceedings of the International Conference for Space Optics (ICSO)*, Toulouse, France, December 5–7, 2000.
12. P. G. Halverson, F. Zhao, R. Spero, S. Shaklan, O. P. Lay, S. Dubovitsky, R. T. Diaz, R. Bell, L. Ames, K. Dutta, "Techniques for the Reduction of Cyclic Errors in Laser Metrology Gauges for the Space Interferometry Mission," *American Society of Precision Engineering Annual Meeting*, Arlington, VA, November 10–15, 2001.
13. L. Ames, et al, "Space Interferometry Mission starlight and metrology Subsystems," *Interferometry in Space*, Vol. 4852, *Proceedings of SPIE*, August 2002.
14. L. Sievers, et al, "Overview of SIM wide angle astrometric calibration strategies", *Interferometry in Space*, Vol. 4852, *Proceedings of SPIE*, August 2002.

SIM Internal Metrology Beam Launcher Development

Feng Zhao*, Rosemary Diaz, Gary Kuan, Norbert Sigrist, and Yuri Beregovski
 Jet Propulsion Laboratory, Pasadena, California 91109
 Lawrence Ames, and Kalyan Dutta
 Lockheed Martin Advanced Technology Center, Palo Alto, California 94304

ABSTRACT

To accomplish micro-arcsecond astrometric measurement, stellar interferometers such as SIM require the measurement of internal optical path length delay with an accuracy of ~ 10 picometers level. A novel common-path laser heterodyne interferometer suitable for this application was proposed and demonstrated at JPL. In this paper, we present some of the experimental results from a laboratory demonstration unit and design considerations for SIM's internal metrology beam launcher.

Keywords: interferometry, metrology, laser heterodyne interferometers, astrometry

1 INTRODUCTION

The Space Interferometry Mission (SIM) is a space-based optical Michelson interferometer with its primary goal of measuring positions and motions of celestial objects. In its simplest form, SIM performs relative astrometry between two stars by taking a pair of internal optical path length delay measurements: one for each star in turn, as shown in Figure 1. The two delay-line positions are located by searching for the maximum fringe amplitude on each star. A key measured quantity is the change in internal delay Δd ,

$$\Delta d = \vec{B} \cdot (\vec{s}_1 - \vec{s}_2),$$

where \vec{B} is the baseline vector (length and orientation) and \vec{s}_1 and \vec{s}_2 are unit vectors to the two stars. The angular distance between the two stars ($\vec{s}_1 - \vec{s}_2$) can then be calculated once Δd and \vec{B} are known. The job of internal metrology is to measure Δd . For SIM, Δd must be measured with an accuracy on the order of 10 picometers in order to achieve 1 microarcsecond astrometry with a 10m baseline.

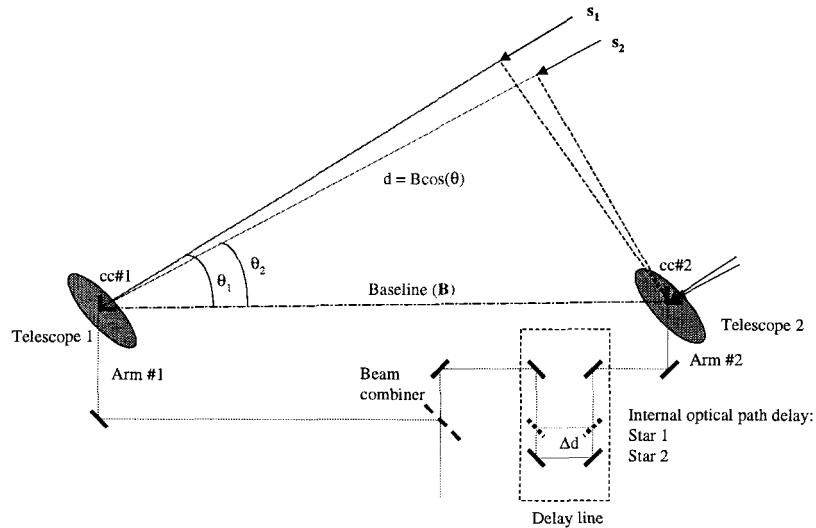


Figure 1. Stellar interferometer for astrometric measurement. The internal delay Δd between two star central fringes gives the angular distance between the two stars.

* Feng.Zhao@jpl.nasa.gov; phone (818)354-3602; fax (818)393-2412, Jet Propulsion Laboratory, M/S 301-486, California Institute of Technology, 4800 Oak Grove Drive, Pasadena, California 91109

Laser heterodyne interferometers have been widely used in high precision displacement measurement and also have been the choice for stellar interferometry for measuring internal path delays [1]. Commercial available heterodyne interferometers are limited to about 1-2nm in linear accuracy [2]. The well-known error term is cyclic error which happens every integer number $\lambda/2$ of displacement in most of the configurations. The cyclic error has been a subject of intensive research [2], and some interesting concepts have been demonstrated to beat the cyclic error down to below 100pm level [3]. However, these concepts are not suited for use in SIM because they are intrinsically sensitive to temperature changes.

A novel COMMON-Path Heterodyne Interferometer (COPHI) was proposed at JPL as a multi-purpose, high resolution laser interferometer [4-6]. Experimental results indicated that very low cyclic error (27pm RMS) and good thermal stability (100pm over one hour) can be obtained at the same time with COPHI [6]. In this paper, we will first describe the COPHI concept and its use as internal metrology beam launcher* for SIM. We will also present some experimental results of one of our laboratory prototypes. In Section 4, we will present some analysis and design work toward a flight internal metrology beam launcher for SIM.

2 COMMON-PATH HETERODYNE INTERFEROMETER (COPHI)

Figure 2 shows COPHI configured as a displacement measuring interferometer for internal path length measurement. It is a laser heterodyne interferometer, where two laser beams with a frequency offset Δf are collimated with stable collimators. One beam is directed to the measurement target with a beam splitter (the top beam at frequency f_o in Figure 2). The interferometer is located at the back end of the astrometric beam combiner, so that the measurement beam passes through the beam combiner and travels toward the star. We place a pair of masks after the beam combiner, one in each arm. The two masks are complimentary, with one selecting only the central portion of the measurement beam, while the other mask selecting an annular part of the beam. As shown in Figure 2, the central beam travels in Arm #2 and the annular beam travels in Arm #1. These two beams are then retro-reflected back to the interferometer by corner cubes #1 and #2, respectively. These two measurement beams are spatially separated with a guard band to reduce cross-talk contamination due to diffraction. The second laser beam (reference beam) at frequency $f_o + \Delta f$, which serves as a local oscillator, then interferes with both measurement beams at the second beam splitter. The two spatially separated fringes are then directed to their own photodiodes with the use of a truncated mirror. The phase difference ($\Delta\phi$) between the reference and measurement signals

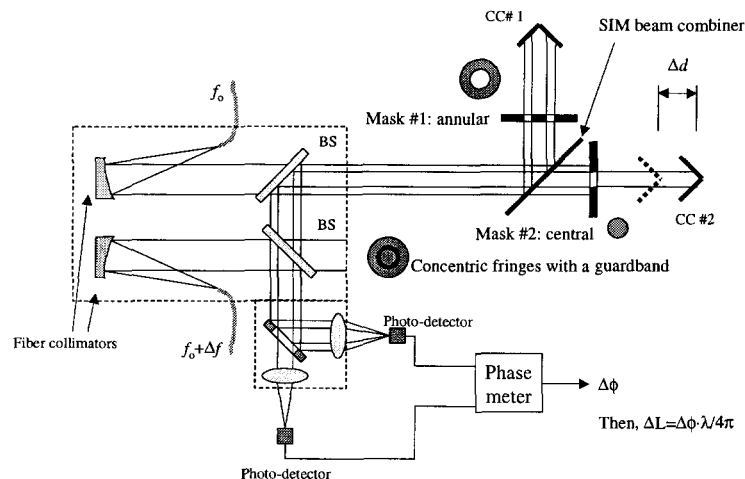


Figure 2. Schematic of a common-path heterodyne interferometer, configured for internal path length measurement.

* The term “beam launcher” refers to laser interferometer for path length measurement in SIM.

is then used to calculate the displacement (Δd) between the fiducials:

$$\Delta d = \frac{\Delta\phi \lambda}{2\pi \cdot 2},$$

where λ is the laser wavelength.

One obvious advantage of using COPHI is that the internal path delay is measured directly with only one interferometer. In conventional internal path length measurement, two interferometers are used to measure the path length in two arms separately [1]. The internal path delay is then the difference of the two measurements. Two sets of phase measurement electronics are needed. The use of COPHI to measure internal path delay reduces the number of beam launchers and the number of phase measurement electronics to only one set.

The second advantage of using COPHI for internal path delay measurement is that the alignment process of the stellar interferometer becomes simpler. To measure the starlight path length accurately, the laser metrology beam and starlight beam must be parallel and the beams from Arm #1 and Arm #2 must be parallel at the astrometric beam combiner, both to be better than 1 μ rad. Since the measurement beams from COPHI are derived from the same collimated wavefront, they are intrinsically parallel. This feature reduces the number of precise alignments in SIM. It also makes it possible to use the COPHI beams as an alignment reference for pointing the two starlight arms.

COPHI also has much smaller nonlinear errors as compared with traditional interferometers. The once largest error source for cyclic error, namely polarization leakage is no longer an issue in COPHI. Since the wavefronts are spatially separated, diffraction may cause crosstalk, thus cyclic error in the measurement. Practically, several simple methods such as baffle to isolate the beams, re-imaging of the mask onto truncated mirror, etc. are quite effective. In addition to these measures, the local oscillator serves as a "spatial filter", which further rejects the contribution of stray light when interfering with the measurement beams. This is because the diffracted beam tends to have a high angular frequency, therefore poor fringe visibility when interfering with a clean local oscillator reference beam. Both analysis and laboratory demonstration have confirmed that the diffraction induced cyclic error can be controlled to 10pm level with a proper guard band between the two wavefront portions. This represents about a factor of 100 in improvement over traditional interferometers.

In COPHI, the wavefront of the measurement beam is split into two symmetric portions, with minimum lateral offset between the two beams. They are referenced to the same reference beam (the local oscillator). The two signals are common-path except that they pass through different parts of the same optics. Therefore, good thermal stability can be achieved without using any compensating optics.

3 LABORATORY DEMONSTRATION

In the last two years, we have designed, built and tested several laboratory prototypes based on COPHI concept for various testbeds [6-9]. In this section, we will describe the SAVV (sub-aperture vertex to vertex) interferometer we developed for the Micro-Arcsecond Metrology (MAM) testbed at JPL.

MAM testbed is part of SIM technology development program aimed at demonstrating micro-arcsecond astrometry, i.e., picometer path length measurement in a laboratory environment. Internal metrology based on traditional polarization type interferometers in MAM has proved to be much more difficult than anticipated [10-12]. SAVV was proposed to address the urgent need for picometer class path length measurement in MAM in late 2000. The first prototype was built with commercial off-the-shelf (COTS) optics.

Figures 3 and 4 show the schematic layout and picture of the first SAVV interferometer. Commercial off-the-shelf doublet collimating lenses are used to collimate the laser beams. To minimize thermal drift error caused by collimator de-spacing, we use a four-quadrant mask pattern, as shown in Figure 5. The collimator de-spacing then becomes a common-mode error, because the measurement beams are on the same radius. The vertical pair and horizontal pair are used in the two arms of the MAM interferometer, selected by a pair of masks shown in Figure 6. Because the diffraction is minimum along the diagonals in the square mask, we select square beam patterns for each beam. Therefore, crosstalk between the vertical and horizontal pairs also becomes minimum. A pair of Risley prisms are used in fine alignment (1 μ rad) of the reference beam (local oscillator) to be parallel to the measurement beams. Two

picomotor rotary stages (New Focus) are used to achieve fine adjustment and also remote alignment to correct for any drift when the interferometer is used in vacuum.

The cyclic error of SAVV was measured with a standard linear long stroke approach, in which one of the two corner cubes was translated with a PZT. The linear path length modulation is much longer than one wavelength, therefore, any cyclic error can be detected by looking at the power spectrum of the displacement result. In our experiment, the laser wavelength is $1.319 \mu\text{m}$, and the total stroke of the PZT is about $40 \mu\text{m}$ with a triangle wave modulation at 0.05Hz . Thus cyclic error with $\lambda/2$ periodicity can be found at about 3.5Hz in the spectral domain.

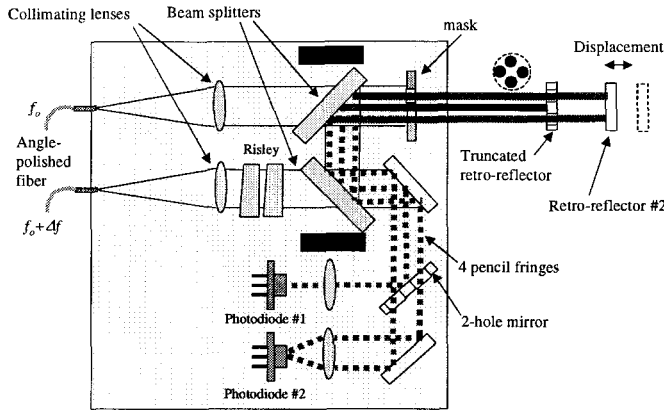


Figure 3. SAVV schematic.

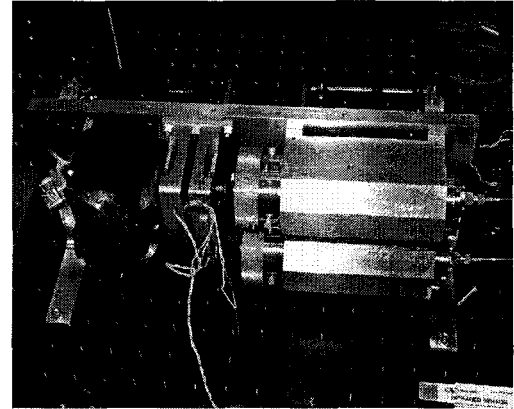


Figure 4. Picture of a SAVV prototype interferometer.

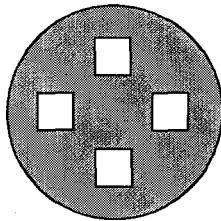


Figure 5. Four square beams are selected from the collimated beam with a quadrant mask in SAVV.

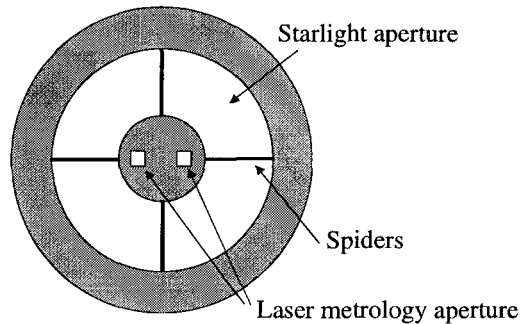


Figure 6. A two-hole mask in Arm #1 selects a horizontal pair of the quadrant beams. In Arm #2, an identical mask rotated by 90° selects the vertical beams. The central obscuration in starlight is used for laser metrology for path delay measurement.

Figure 7-a shows the measured displacement of the PZT. We select an arbitrary linear displacement, e.g., between 44 and 61 seconds in Figure 7 for analysis. Figure 7-b shows its residual after removing its linear to 4^{th} order terms. The power spectral density of the residual is calculated and plotted in Figure 8-a, in which the peak at 3.8Hz indicates the existence of $\lambda/2$ periodic nonlinear error. The total energy of this cyclic error is estimated to be about 4500pm^2 , which translates into a periodic nonlinear error of only 67pm RMS (figure 8-b). This result exceeds MAM's requirement for 100pm cyclic error.

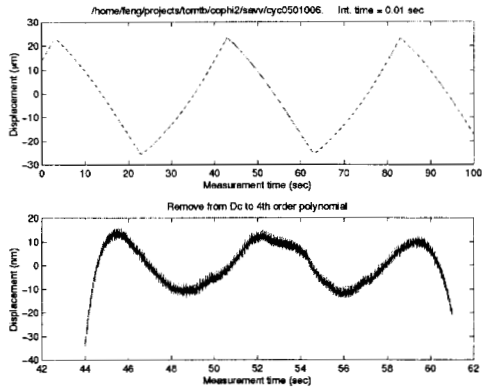


Figure 7. Linear displacement over many laser wavelengths to detect cyclic error in SAVV. The bottom plot shows the residual after removing its DC to 4th order polynomial terms.

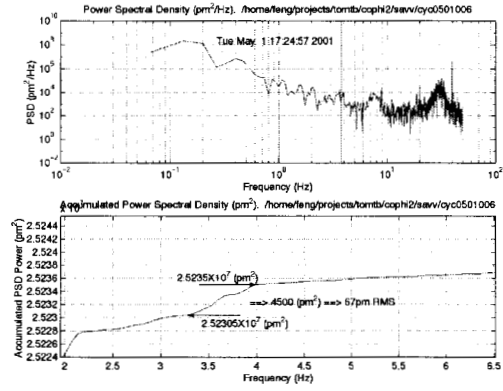


Figure 8. Power spectral density of Figure 7-b. The peak at 3.8Hz is attributed to SAVV cyclic error. The accumulated PSD data (bottom) indicates the cyclic error is about 67pm RMS.

The cyclic error measurement result was then checked against wave optics diffraction model. In the model, the diffraction effects of both beams at various mask apertures are calculated. Diffraction results in cross-talk between the two photo detectors, which in turn causes error in average phase of each signal. The calculated cyclic error in the SAVV measurement setup is plotted in Figure 9. The calculations indicate that the cyclic error of SAVV beam launcher is less than 10 pm RMS. The difference between the measurement and calculation may be attributed to other sources of cyclic error such as electronics cross-talk between the two signals, fiber tip back scattering causing a contamination of the two measurement beams, and alignment errors in SAVV.

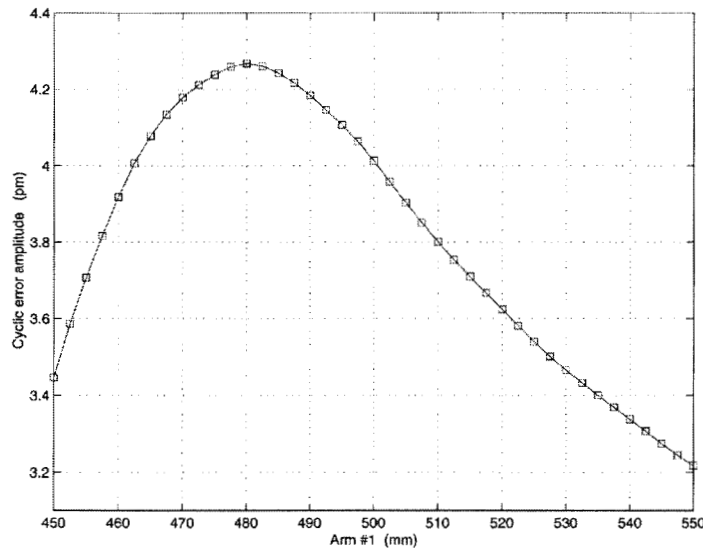


Figure 9. Calculated cyclic error for the SAVV measurement setup. This calculation assumes perfect alignment and considers only the effect of diffraction.

SAVV's temperature sensitivity was measured, using the lab ambient temperature fluctuation (~1°C) as a source to drive SAVV temperature. In the measurement, a corner cube was placed in front of SAVV, all four beams are reflected from this corner cube. Sending all the measurement beams to the same

corner cube ensures no path length drift in the fiducial. Thus, any errors in the readout can be attributed to the interferometer. The thermal stability results are shown in Figures 10 and 11. The results indicate that SAVV even built with COTS, has a good thermal stability, less than 4nm/K at room temperature. It can also be seen from Figure 10 that, SAVV drift is highly correlated with the change in temperature gradient. Gradient fluctuations in the middle of the measurement were caused by the air conditioning on/off in the lab. The flight environment will not have this type of temperature fluctuations.

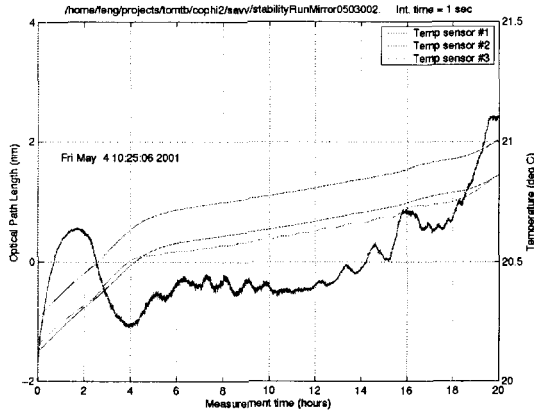


Figure 10. SAVV drift vs. bulk temperature.

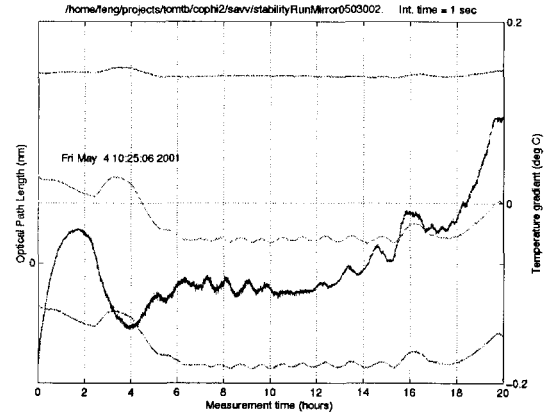


Figure 11. SAVV drift vs. temperature gradient.

4 DESIGN CONSIDERATIONS FOR SIM

The COPHI concept has been successfully demonstrated in ground testbeds and it has been selected as the baseline concept for SIM flight internal metrology. In this section, we will present some of the design considerations for a flight SIM internal metrology interferometer.

One of the differences between ground testbeds (e.g., MAM) and SIM is the total path length that metrology beams and starlight travel. In MAM, the star light path length is 5 meters, and in SIM the path length is about 10-20 meters. In addition, there will be a beam compressor in SIM, where the metrology beam will be magnified by 7 \times . Due to diffraction over long path lengths, the metrology beam expands and requires a relatively large corner cube on the siderostat (SID). On the other hand, a small corner cube is preferred to meet the starlight throughput requirement. Therefore, the flight internal metrology beam size becomes an important aspect of the SIM beam launcher design.

In addition to the beam size constraints set by the corner cube size, the throughput is also an important issue. The four-quadrant beam configuration in MAM internal metrology has the drawback of low light efficiency, since only a few percent of the light is used in the four-quadrant from the collimated beam.

In SIM internal metrology, we plan to use the COPHI configuration, with concentric beams, an annulus and a core, as we described in Section 2 in Figure 2. The layout of SIM internal beam launcher is shown in Figure 12. Low thermal expansion materials such as Zerodur or ULE are used to make the collimator optics (off-axis parabolas and spacers) to ensure thermal stability of the collimated beams. De-spacing of the collimator will cause a focus error in the wavefront, thus an error between the core and annular beams. To some extent, this is a common-mode error, since both collimators will experience similar amount of de-space to thermal soak fluctuations.

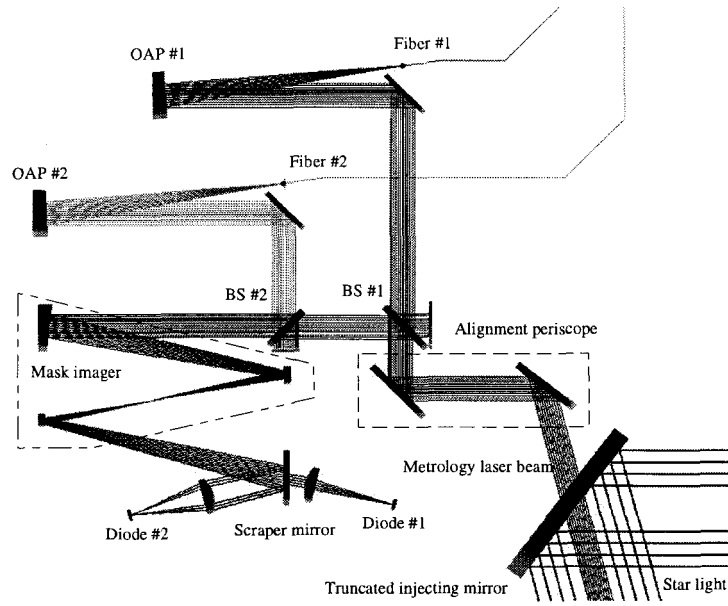


Figure 12. Schematic of internal metrology beam launcher for SIM. The astrometric beam combiner optic and the masks that separate the measurement beams into core and annulus portions are at the lower right corner (not shown).

The SIM internal metrology launcher is located inside of the Astrometric Beam Combiner (ABC), where a truncated mirror behind the main beam combiner optics is used to inject the internal metrology measurement beams into the starlight optics train [13]. The truncated mirror reflects the annular starlight to the starlight camera. A pair of alignment mirrors (periscope) are used to align the metrology beam with the starlight, both in pointing and in overlap. It is much easier to actuate the alignment mirrors than to actuate the beam launcher or starlight optics. After the metrology measurement beam enters the main beam combiner, the beam is then spatially selected into a core beam and an annulus beam separately into two starlight arms with the use of a pair of concentric masks. These two spatially separated beams then propagate along each arm of the starlight optics. Upon reflecting off the corner cubes, the two measurement beams return to the ABC and enters internal beam launcher. The local oscillator beam (fiber #2) is aligned with both the core and annulus measurement beams at the second beam splitter (BS #2). Before the two measurement beams are combined at the beam combiner, they propagate independently in each arm of SIM. The beam diffraction does not introduce cross-talk between them. After returning to the masks at the beam combiner (ABC), the two measurement beams co-propagate and diffraction will cause cross-talk. This happens only between the masks and the scraper mirror, which we use to separate the two fringes. To beat the cyclic error down to the 10pm level, one needs the cross-talk to be less than -80dB . To “reverse” the diffraction effect, we use an imaging system whose two conjugates are the masks and the scraper mirror. By using the imaging approach, the two fringes are separated with smaller cross-talk, thus lower cyclic error. In Figure 12, the “mask imager” is a 3-element, all-spherical, reflective, $1\times$ imaging system. The effects of aberration, aperture, and scattering to fringe cross-talk are now under detailed study.

As mentioned previously, the SID corner cube clear aperture places an upper limit on the metrology beam diameter. If one collimates the measurement beam to infinity, then the beam diameter may be larger than the corner cube. In the SIM internal metrology launcher, we propose to “focus” the laser beams on the SID corner cube. In other words, instead of collimating the laser beams to infinity (finite-to-infinite conjugates), we align the fibers in the collimator to form finite-to-finite conjugates. By doing so, the beam waist where the smallest beam diameter occurs is located at the SID corner cube. Figures 13 and 14 shows an example of beam profiles at different locations. The path length used in this calculation is 8m single-pass. The final path length in SIM is yet to be defined. From the plots, we can see that the core beam

has less diffraction rings, whereas the annulus beam has more diffraction rings due to the inner and out apertures. Both the core and annulus beams have a smaller footprint on the SID corner cube. Upon returning back to the ABC, the diffraction rings are cleaned up by the masks at the beam combiner (ABC). With the use of mask imager, the beam profiles at the scraper mirror look nice and clean (Figure 15).

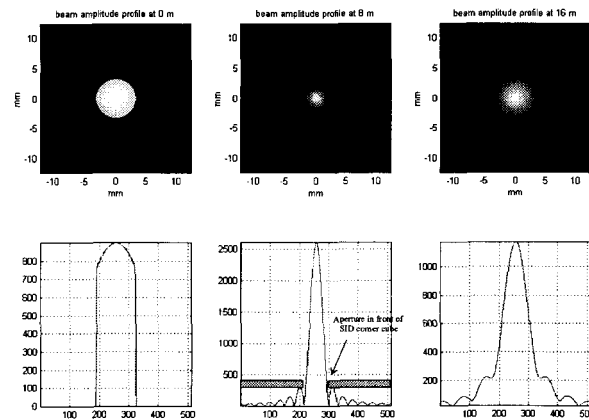


Figure 13. Beam intensity profiles of the core beam at several distances. Left: after the ABC masks traveling to SID. Center: at the SID. Note the clear aperture of the corner cube selects only the central portion of the diffracted beam. Right: back to the ABC masks after a round trip.

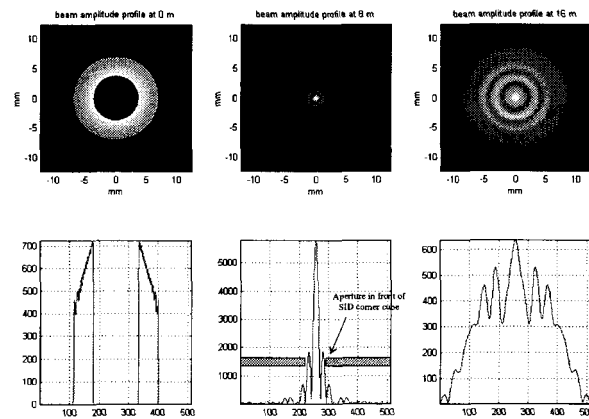


Figure 14. Beam intensity profiles of the annulus beam at several distances. Left: after the ABC masks traveling to SID. Center: at the SID. Note the annulus beam focuses into a smaller spot on SID corner cube. Right: back to the ABC masks after a round trip.

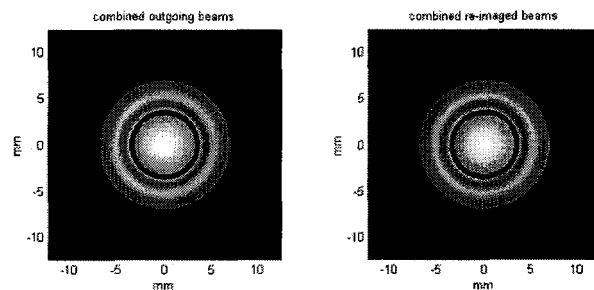


Figure 15. Co-propagating core and annulus beams. Left: after the round trip and combined at the astrometric beam combiner. Right: image at the scraper mirror with the use of mask imager.

The effect of using “finite-to-finite” conjugate ratio in the collimator has a large impact on the beam size on SID corner cube. It allows us to use smaller corner cube on SID, thus improve the starlight throughput. Then the question arises: does the focused beam introduce any error in the average phase in the metrology beam as the path length varies? To answer this question, we have calculated the effect using wave optics diffraction model. The analysis results are plotted in Figure 15, where for both cases, focused and unfocused, there is a quasi-linear deviation from geometric distances. The deviation from geometric case is caused by the fact that both beams have finite beam sizes, thus diffraction occurs in both focused and unfocused beams. This diffraction-induced term in path length measurement is a subject of other papers [14], and readers are referred to the calibration of this term for SIM. In Figure 15, the two traces for focused and unfocused beams have some differences, but there is no effect on how the calibration will be carried out in SIM.

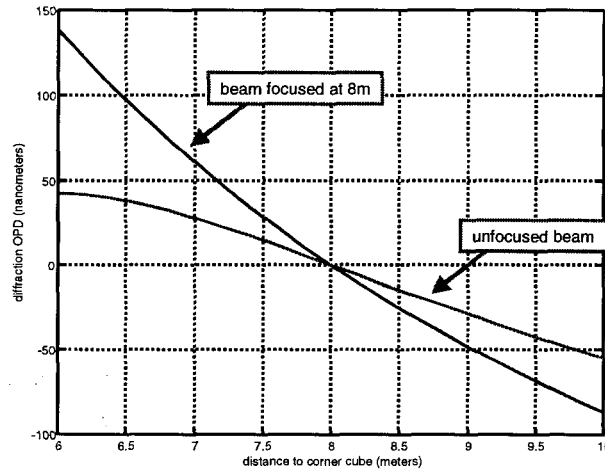


Figure 16. Deviation from geometric distances due to diffraction in both focused and unfocused measurement beams. The horizontal axis represents the internal delay positions.

5 SUMMARY

We have developed and demonstrated an internal metrology beam launcher concept for the Space Interferometry Mission. The concept is based on common-path heterodyne interferometer (COPHI) developed at JPL. The use of spatial separation of measurement beams significantly reduces the cyclic error. Experimental results from laboratory demonstration units have shown encouraging results (cyclic error ~ 67 pm RMS). Calculations based on wave optics diffraction model also indicate that the diffraction in spatially separated measurement beams results in ~ 10 pm level cyclic error. We have also identified a simple approach to reduce the beam sizes over long distances due to diffraction.

ACKNOWLEDGEMENT

The authors would like to thank Jeff Oseas for his help on creating the Light Tool model of the internal metrology beam launcher. This work was carried out at the Jet Propulsion Laboratory, California Institute of Technology, under a contract with the National Aeronautics and Space Administration.

REFERENCES

1. M. Shao, M. M. Colavita, B. E. Hines, D. H. Staelin, D. J. Hutter, K. J. Johnson, D. Mozurkewich, R. S. Simon, J. L. Hersey, J. A. Hughes, and G. H. Kaplan, “Mark III Stellar Interferometer,” *Astron. Astrophysics*, **193**, pp. 357–371, 1988.
2. N. Bobroff, “Recent advances in displacement measuring interferometry”, *Meas. Sci. Technol.*, vol. 4, pp. 907-926, 1993.

3. C.-M. Wu, J. Lawall, R. D. Deslattes, "Heterodyne Interferometer with Subatomic Periodic Nonlinearity", *Appl. Opt.*, Vol. 38, Issue 19, pp. 4089-4094, 1999.
4. F. Zhao, "A common-path, multi-channel heterodyne interferometer," *NASA Tech. Briefs*, Vol. 25, No. 7, pp12, 2001.
5. F. Zhao, "Interferometric apparatus for ultra-high precision displacement measurement", US Patent Pending, NASA Case No. NPO-21221-1-CU, 2001.
6. F. Zhao, "Demonstration of sub-Angstrom cyclic nonlinearity using wavefront-division sampling with a common-path laser heterodyne interferometer", *Proceeding of the American Society for Precision Engineering (ASPE) Annual Meeting*, Crystal City, VA, 2001.
7. F. Zhao, J. Logan, S. Shaklan, and M. Shao, "A common-path, multi-channel heterodyne laser interferometer for sub-nanometer surface metrology," *Proc. SPIE*, Vol. 3740, pp 642-645, 1999.
8. F. Zhao, R. T. Diaz, P. G. Halverson, G. M. Kuan, and S. Shaklan, "Wavefront versus amplitude division high precision displacement measuring interferometers," *Proceedings of Optoelectronic Distance/Displacement Measurements and Applications (ODIMAP II)*, Pavia, Italy, September 20–22, 2001.
9. F. Zhao, R. T. Diaz, P. Dumont, P. G. Halverson, S. Shaklan, R. E. Spero, L. Ames, S. Barrett, R. Barrett, R. Bell, R. Benson, G. Cross, K. Dutta, T. Kvamme, B. Holmes, D. Leary, P. Perkins, M. Scott, and D. Stubbs, "Development of Sub-nanometer Racetrack Laser Metrology for External Triangulation Measurement for the Space Interferometry Mission," *American Society of Precision Engineering Annual Meeting*, Arlington, VA, November 10–15, 2001
10. A. Kuhnert, S. Shaklan, Y. Gursel, S. Azevedo, and Y. Lin, "Metrology for the micro-arcsecond metrology testbed," *Proceedings of SPIE conference on Astronomical Interferometry*, Vol. 3350, pp. 571–587, 1998.
11. P. G. Halverson, A. Kuhnert, J. Logan, M. Regher, S. Shaklan, R. Spero, F. Zhao, T. Chang, R. Gutierrez, E. Schmitdlin, T. Vanzandt, J. Yu, "Progress toward picometer accuracy laser metrology for the Space Interferometry Mission," *Proceedings of the International Conference for Space Optics (ICSO)*, Toulouse, France, December 5–7, 2000.
12. P. G. Halverson, F. Zhao, R. Spero, S. Shaklan, O. P. Lay, S. Dubovitsky, R. T. Diaz, R. Bell, L. Ames, K. Dutta, "Techniques for the Reduction of Cyclic Errors in Laser Metrology Gauges for the Space Interferometry Mission," *American Society of Precision Engineering Annual Meeting*, Arlington, VA, November 10–15, 2001.
13. L. Ames, et al, "Space Interferometry Mission starlight and metrology Subsystems," *Interferometry in Space*, Vol. 4852, *Proceedings of SPIE*, August 2002.
14. L. Sievers, et al, "Overview of SIM wide angle astrometric calibration strategies", *Interferometry in Space*, Vol. 4852, *Proceedings of SPIE*, August 2002.